Int J Appl Earth Obs Geoinformation 68 (2018) 252–261

Contents lists available at ScienceDirect

Int J Appl Earth Obs Geoinformation

journal homepage: www.elsevier.com/locate/jag

Evaluating the impact of sea surface temperature (SST) on spatial distribution of chlorophyll-*a* concentration in the East China Sea

Chenxu Ji[a], Yuanzhi Zhang[a,b,*], Qiuming Cheng[c,**], JinYeu Tsou[b], Tingchen Jiang[d], X. San Liang[a]

[a] Nanjing University of Information Science and Technology, School of Marine Sciences, Nanjing, 210044, China
[b] Chinese University of Hong Kong, Center for Housing Innovations, Shatin, Hong Kong
[c] China University of Geosciences, State Key Laboratory for Geological Processes and Mineral Resources, Beijing, 100083, China
[d] Huaihai Institute of Technology, Faculty of Surveying and Mapping, Lianyungang, 222005, China

ARTICLE INFO

Keywords:
Sea surface temperature (SST)
Chlorophyll-*a* concentration (Chl-a)
The East China Sea (ECS)
DINEOF
MODIS data

ABSTRACT

In this study, we analyze spatial and temporal sea surface temperature (SST) and chlorophyll*a* (Chl-a) concentration in the East China Sea (ECS) during the period 2003–2016. Level 3 (4 km) monthly SST and Chl-a data from the Moderate Resolution Imaging Spectroradiometer Satellite (MODIS-Aqua) were reconstructed using the data interpolation empirical orthogonal function (DINEOF) method and used to evaluated the relationship between the two variables. The approaches employed included correlation analysis, regression analysis, and so forth. Our results show that certain strong oceanic SSTs affect Chl-a concentration, with particularly high correlation seen in the coastal area of Jiangsu and Zhejiang provinces. The mean temperature of the high correlated region was 18.67 °C. This finding may suggest that the SST has an important impact on the spatial distribution of Chl-a concentration in the ECS.

1. Introduction

As the largest epicontinental sea in the western Pacific Ocean (Jiao et al., 2007), the East China Sea (ECS) has a broad continental shelf area of about 5×10^5 km^2 (Gong et al., 2003). It is connected to the Pacific Ocean, the South China Sea, the Sea of Japan, and the Yellow Sea by a very complex ocean system having both deep and shallow sea features. Situated east of China, it is of undeniable value to the nation, for its characteristics affect the entire coastal region (Johnson and Toy, 2017).

Being characterized by the variable seasonal river runoff and a wide continental shelf, the ECS is highly dynamic (Zhang et al., 2007; Siswanto et al., 2008). The Yangtze River discharge brings both nutrients and fresh water to the ECS in abundance but has heightened levels of dissolved inorganic nitrogen since the 1980s (Xu et al., 2013; Gong et al., 1996). Some researchers reported that the Yangtze River discharge can affect upper-ocean stratification and thereby contributes to a reduction in summer SST in the ECS (Kako et al., 2016; Gong and Wong, 2017; Zhang et al., 2017). The correlation between SST and Chl-a was significant at a certain temperature (Kavak and Karadogan, 2011). However, excessive temperature would inhibit the increase of Chl-a concentration (Nurdin et al., 2013). It is also found that when the seasonal river discharge is high (low), correlation between SST and chlorophyll is positive (negative) in the coastal Bay of Bengal region (Jutla et al., 2011).

According to the previous studies, the SST of ECS had experienced a significant warming trend during the past four decades (Tang et al., 2009; Bao and Ren, 2014). The SST of ECS has obviously seasonal and interannual changes (Bao and Ren, 2014). Summing up the distribution of SST in the ECS, it is noted that the isotherms are mostly parallel to isobaths, running in the southwest-northeast direction (Tseng et al., 2000).

As a biological parameter, Chl-a concentration reflects an abundance of phytoplankton. By observing it, we can monitor conditions favorable to red tide, cyanobacteria, and other causes of marine biological disaster (Steidinger and Haddad, 1981; Tomlinson et al., 2004). According to the previous studies (Thomas et al., 2001; Gong et al., 1996), many factors could affect the Chl-a concentration (Tran et al., 1993). For example, the Kuroshio Current can affect Chl-a concentration, in the core of cyclonic (or anticyclonic) eddies in the Kuroshio Extension, the high (or low) area-averaged Chl-a concentrations often occured (Shinya et al., 2016), and cold-core (cyclonic) rings correspond to areas of high Sea-Viewing Wide Field-of-View Sensor (SeaWiFS) Chl-a. Warm-core (anticyclonic) rings relate to the areas of low Chl-a concentration (Chu and Kuo, 2009).

Barber and Chavez (1983) have conjectured that the levels of nutrients and phytoplankton biomass and primary productivity are clearly

* Corresponding author at: Nanjing University of Information Science and Technology, School of Marine Sciences, Nanjing, 210044, China.
** Corresponding author.
E-mail addresses: jichenxu@nuist.edu.cn (C. Ji), yuanzhizhang@cuhk.edu.hk (Y. Zhang), qiuming.cheng@iugs.org (Q. Cheng), jiangtc@hhit.edu.cn (T. Jiang).

https://doi.org/10.1016/j.jag.2018.01.020
Received 2 November 2017; Received in revised form 13 January 2018; Accepted 31 January 2018

regulated by the physical changes brought on by El Niño. Subsequently, many researchers have confirmed the relationship between phytoplankton variability and the El Niño–Southern Oscillation (ENSO) (Nakamoto et al., 2001; Park et al., 2011), with some studies reporting that surface Chl-a concentrations were associated with the 1997–1998 and 2015–2016 El Niño events (Mati and Mitchell, 2000; Jacox et al., 2016). Because of the eastward zonal advection of upper ocean currents, two types of El Niño events (Cold Tongue El Niño and Warm Pool El Niño) can produce anomalous Chl-a concentrations (Lee et al., 2014).

Some researchers have investigated the relationship between Chl-a concentration and SST for a particular sea area. In the ECS, for example, the SST has great effect on the red tide with the correlation coefficient reached 0.707 (Yang and He, 2009). With the increase in SST, the Chl-a showed a decrease in the Zhejiang coastal waters (Wang et al., 2010). In comparison, in the Black Sea, their correlation was estimated to be 60% (Kavak and Karadogan, 2011). However, in the Spermonde Indonesia region, an inverse correlation was reported, with the coefficient of correlation at $R = 0.542$ (Nurdin et al., 2013). There is an inverse relationship at most of the locations of the Arabian Sea during January to April, while the northwest region shows a positive relationship during October to December (Chaturvedi, 2005). The time series of SST and Chl-a for coastal and offshore regions have been compared in some studies, and they found that for offshore region, it was usually inverse relationship, but a positive relationship is observed between them in coastal waters which have high river discharge (Jutla et al., 2011). According to the researches of Colwell (1996) and Lobitz et al. (2000), the phytoplankton and SST presented a positive relationship.

Hampered as they are by limited data, however, researchers have rarely looked at seasonal variations of SST and Chl-a concentration, and the relationship between the two, throughout the entire ECS shelf. Most published papers have used in situ data, which is precise but incomplete and is limited to the time. Herein, we reconstructed Moderate Resolution Imaging Spectroradiometer Satellite (MODIS-Aqua) data using the data interpolation empirical orthogonal function (DINEOF) method, which fills in missing data from geophysical fields (Beckers and Rixen, 2003), just as Miles and He (2010) took a DINEOF-based approach to reconstructing MODIS data for the South Atlantic Bight so as to analyze the characteristic and variance of SST and Chl-a.

In this paper, we aim to reconstruct and analyze the major features of seasonal and interannual variability in Chl-a concentration and SST in the ECS. We also want to examine the corresponding characteristics of Chl-a spatial distribution and to assess the SST's impact on it.

2. Data and methods

2.1. Data sets

The SST and Chl-a concentration data were derived from MODIS-Aqua measurements, downloading from the oceancolor website (https://oceancolor.gsfc.nasa.gov/) Level 3 (4 km) monthly data of SST and Chl-a for the period from January 2003 to December 2016. All the data were applied to our study area in the ECS at 117°–130°E and 23°–36°N (see Fig. 1).

2.2. Methods

2.2.1. The data interpolation empirical orthogonal function method

DINEOF is an empirical orthogonal functions (EOF)-based method for filling in data missing from geophysical fields. We now briefly describe the DINEOF processing procedure (Beckers and Rixen, 2003; Alvera-Azcárate et al., 2005):

First, we recombine the raw data into a matrix of dimensions' m × n, where m is the number of space points and n is the months'. Both original and missing data are contained in the matrix. Then we randomly put 1% of the existing data into another matrix X^e to conduct cross-validation. After that, we subtract the average temporal value of the matrix and use MATLAB's interp2 function to set the missing data using the interpolating prediction value of each month (including cross-validation data).

Step 1: By applying the singular value decomposition (SVD) to the matrix, the spatial EOFs (U), temporal EOFs (V), and the singular values matrix (S) is got:

$$X = USV^T \tag{1}$$

Step 2: We can then reconstruct the missing data using the formula:

$$X_{i,j}^{re} = \sum_{k}^{p=1} S_p (U_p)_i (V_P^T) \tag{2}$$

Where $X_{i,j}^{re}$ is the missing data; i, j are the spatial and temporal indices of the missing data; k is the number of the EOF's mode; U_p and V_p are the pth column of the spatial and temporal EOFs; and S_p is the singular value.

Step 3: We can get a new matrix without missing data using Eq. (1), where $k = 1$. Then the root mean square error (RMSE) was calculated at the cross-validation points using the mathematical expression

$$R = \sqrt{\frac{1}{N} \sum_{N}^{t=1} (X_t - X_t^e)^2} \tag{3}$$

where N is the points of cross-validation matrix.

Step 4: Then we reconstruct the matrix using the formula:

$$X^{re} = X + \alpha X \tag{4}$$

Where αX is the correction matrix of the missing points (the points that do not affect the observed ones). Then we perform step 1 to get U, V, and S, iterating this process until the predefined convergence criterion was reached and the value of R stabilized (the threshold value of 1×10^{-4}).

Step 5: Increase the number of reconstructed EOFs (k) from 2 to k_{max}, with steps 1–4 repeated until we get the minimum R. Meanwhile, the corresponding value of k can be obtained.

Step 6: We reconstruct the raw data with the value of k obtained in step 5 (Wang and Liu, 2014).

2.2.2. Correlation analysis

In statistical analysis, the Pearson correlation coefficient is used to evaluate for a linear relationship between selected variables of the data. The expression is given by Pearson (1895) as

$$r = \frac{1}{n-1} \sum_{n}^{i=1} \left(\frac{X_i - \overline{X}}{S_x} \right) \left(\frac{Y_i - \overline{Y}}{S_y} \right) \tag{5}$$

where n is the sample size and r lies between -1 and 1, with 1 signifying total positive linear correlation, 0 no linear correlation, and -1 total negative linear correlation. It should be noted that there is no causal link between the value of r and the degree of correlation. If $r = 0$, there is no linear relationship between variables. But they may be connected by other ways; a t-test can be carried out to judge the relevant level.

All the data have been preprocessed before calculating the correlation coefficient. Before analyzing Chl-a and SST time series correlation, we preprocessed the data with the function 'detrend' in the MATLAB. This function can subtract the mean or a best-fit line (in the least-squares sense) from raw data. By removing the trend from the data, it enables us to focus our analysis on the fluctuations in the data about the trend. This method eliminated residual wiggles associated with imperfect sampling of annual variations in the absence of significant annual variation (Hartmann and Michelsen, 1989).

2.2.3. Calculation of standardization index

To compare an observation to a standard normal deviate, the data were standardized using the Z-SCORE method. The method is based on

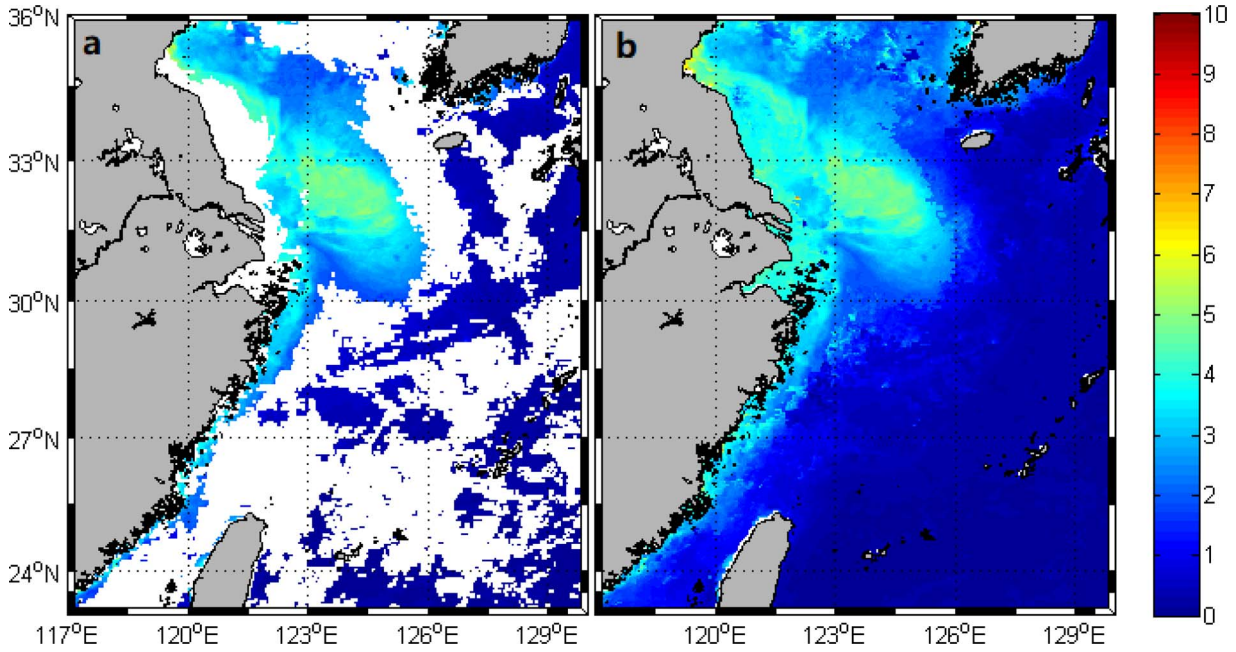

Fig. 1. The original (a) and DINEOF (b) Chl-a concentration of January 2016 (units: mg/m^3).

the data mean and standard deviation for data standardization, which is called the anomaly index and is calculated by (Zill et al., 2011):

$$K_i = \frac{X_i - \overline{X}}{S} i = 1,2,3, \ldots\ldots\ldots,n \tag{6}$$

Where $\overline{X}$ is the mean of the population and S is the standard deviation of the population.

If the absolute value of K_i lies between 0.1 and 1, it is in the normal range, representing the distance between the raw score and the population mean in units of the standard deviation. If it is greater than 1, then it is abnormal. If it is greater than 2, then the datum far exceeds the average value. If it is less than -1, it is on the low side.

2.2.4. Mann–Kendall test

Mann–Kendall (MK) test, a nonparametric test used to statistically identify a monotonic trend in the variable of interest over time, even if there is a seasonal component in the series. In the parametric linear regression analysis, the MK test can be used to test whether the estimated linear regression line's slope is different from zero (Mann, 1945; Kendall, 1975). The computational procedures are as follows (Yue and Wang, 2004):

First, the MK statistic, S, is defined as:

$$S = \sum_{n-1}^{i=1} \sum_{n}^{k=i+1} sgn(x_k - x_i) \tag{7}$$

Where, x_k and x_i are the annual values in years' k and i, and k > i, respectively.

Then, the statistic S is approximately normally distributed when n ≥ 8, with the variance as follows:

$$var[S] = \left[n(n-1)(2n+5) - \sum_t t(t-1)(2t+5) \right] /18 \tag{8}$$

where t is the number of observations. The summation term in the numerator is used only if the data series contains tied values.

Finally, the test statistic Z_c is used as a measure of the significance of a trend and it is given by:

$$Z_c = \begin{cases} \frac{S-1}{\sqrt{var(S)}}, S > 0 \\ 0, S = 0 \\ \frac{S+1}{\sqrt{var(S)}}, S < 0 \end{cases} \tag{9}$$

A positive and negative Z_c values indicate an upward and downward trend, respectively. When $|Z_c| > 1.64$, it represents that the trend is at the significance level of 0.05 in this study.

3. Results and discussion

3.1. The variation of chla concentration and SST

We selected the ECS of 117°–130°E and 23°–36°N as the study area. The ability of the DINEOF to reconstruct the missing Chl-a and SST is demonstrated in Figs. 1 and 2. The cross-validation RMSE of the SST DINEOF reconstruction is 0.4694; for Chl-a, it is 0.5978. The raw Chl-a covered only a part of the ECS, for the nearshore data were almost missing (Fig. 1a). The DINEOF Chl-a (Fig. 1b), however, presented a complete structure for the Chl-a concentration, effectively making up the missing data.

To verify the credibility of the reconstructed data, we compared it with the measured data of August 2011 (adopted from Fei et al., 2012). The obtained result shows that the reconstructed Chl-a has a same distribution as the measured Chl-a in the August of 2011. Especially in the Yangtze River Estuary and the east of the Hangzhou Bay, their Chl-a spatial distribution agrees well between the filled data and the in-situ data.

Similarly, the DINEOF reconstructed the SST's distribution in the study area. It can be seen from Fig. 2 that the spatial SST's distribution is expected, for example, the blank area of SST in the north of Taiwan in Fig. 2a to be produced in Fig. 2b.

In the ECS, we first computed the mean of the original and reconstruction field to gain a variation curve for Chl-a concentration during the period 2003–2016. Fig. 3 shows the changes in Chl-a concentration from 2003 to 2016, with the blue curve representing the original data and the yellow one the results of reconstruction. Chl-a concentration as reconstructed is higher than seen in raw data, perhaps as the result of higher nearshore Chl-a concentrations. Even so, it is clear that both of the curves have the same trend of fluctuation. From

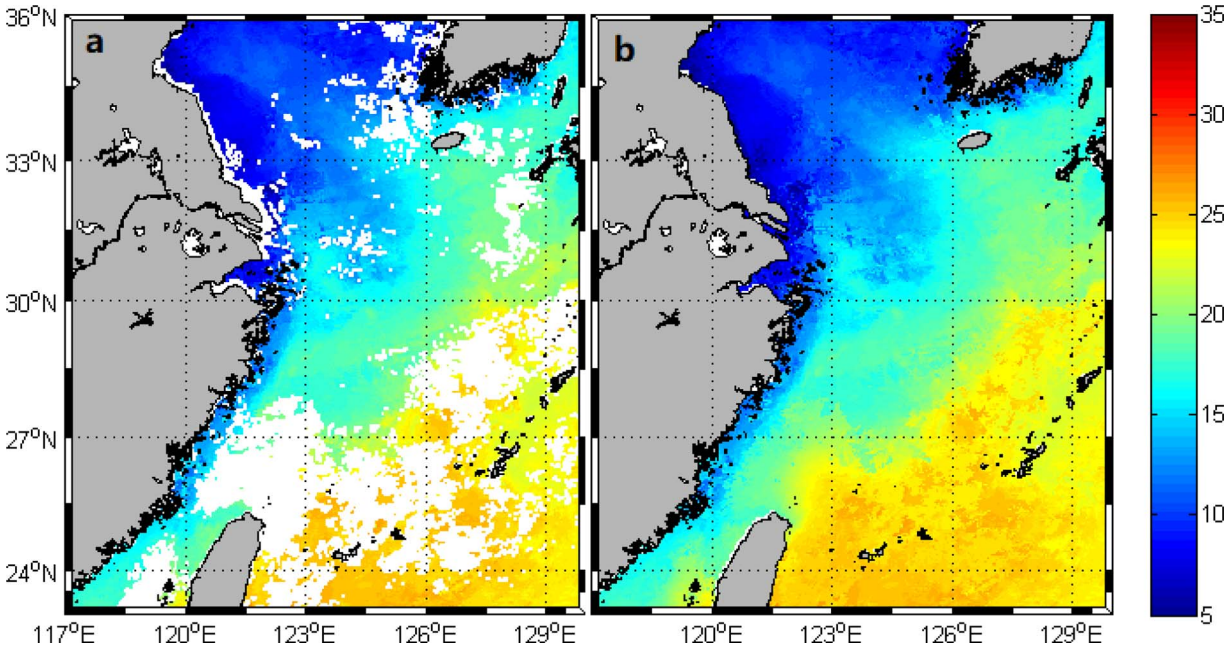

Fig. 2. The original (a) and DINEOF (b) SST of January 2016 (unit: °C).

the DINEOF monthly average curve, we can see that Chl-a concentration reached a peak in April–May and declined to its low point in July–August or, sometimes, October–November. Peaks seen in 2009, 2010, 2012, and 2014 coincided with El Niño (Nakamoto et al., 2001; Park et al., 2011).

Then, the yearly mean of the concentration were calculated (Fig. 4), with blue representing original data and yellow for reconstructed data. As evident from Fig. 4, the Chl-a value showed a fluctuating upward trend from 2003 to 2010, but down to 1.3 mg/m^3 in 2013. For the latest three years, it maintained a high value of about 1.4 mg/m^3. On the whole, yearly mean Chl-a concentration exhibited an uptrend, passing the M-K test with a value of 2.3 (> 1.64) at the confidence of 95%, meaning that the trend was significant, which is consistent with a previous result (Kavak and Karadogan, 2011).

Using Eq. (2), the standard score of the whole monthly reconstruction of Chl-a concentration during the period of 2003–2016 for

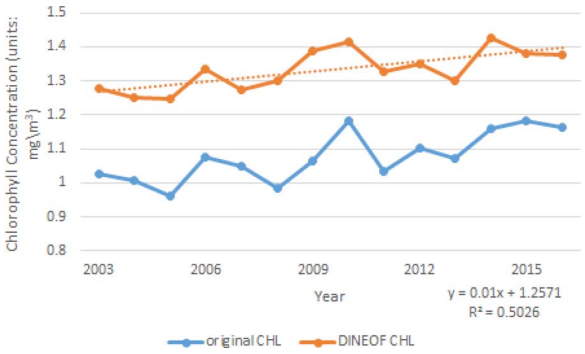

Fig. 4. Yearly mean of Chl-a concentration from 2003 to 2016 (Z_c (DINEOF Chl-a) $| > 1.64$, the trend is significant, passing the M-K test with the confidence of 95%).

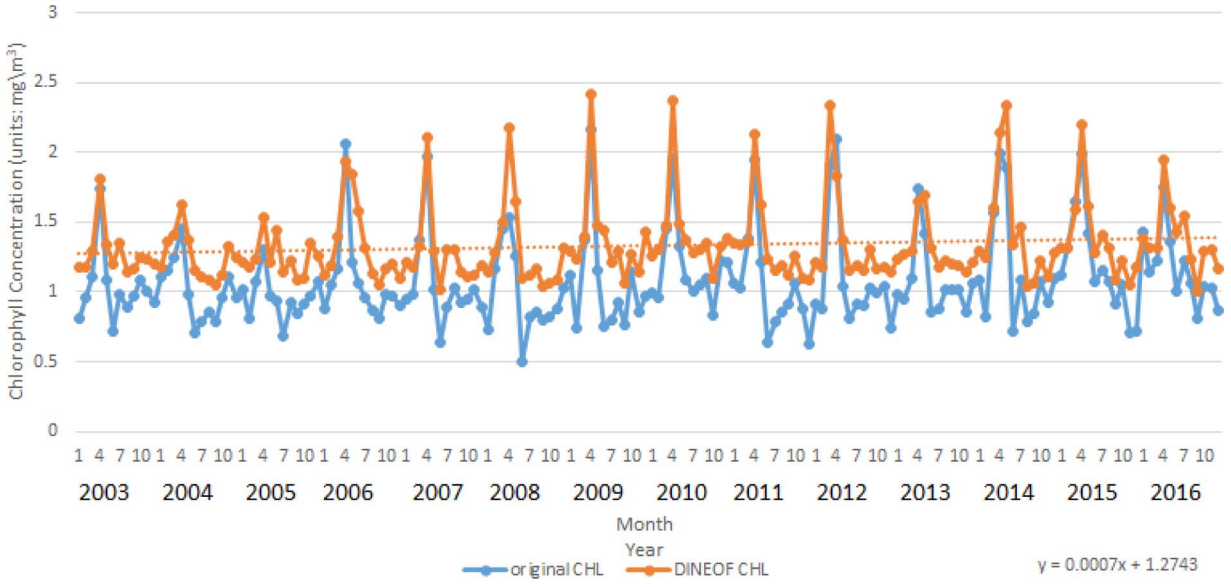

Fig. 3. Long-term changes of Chl-a concentration from 2003 to 2016 (Z_c (DINEOF Chl-a) $| > 1.64$, the trend is significant, passing the M-K test with the confidence of 95%).

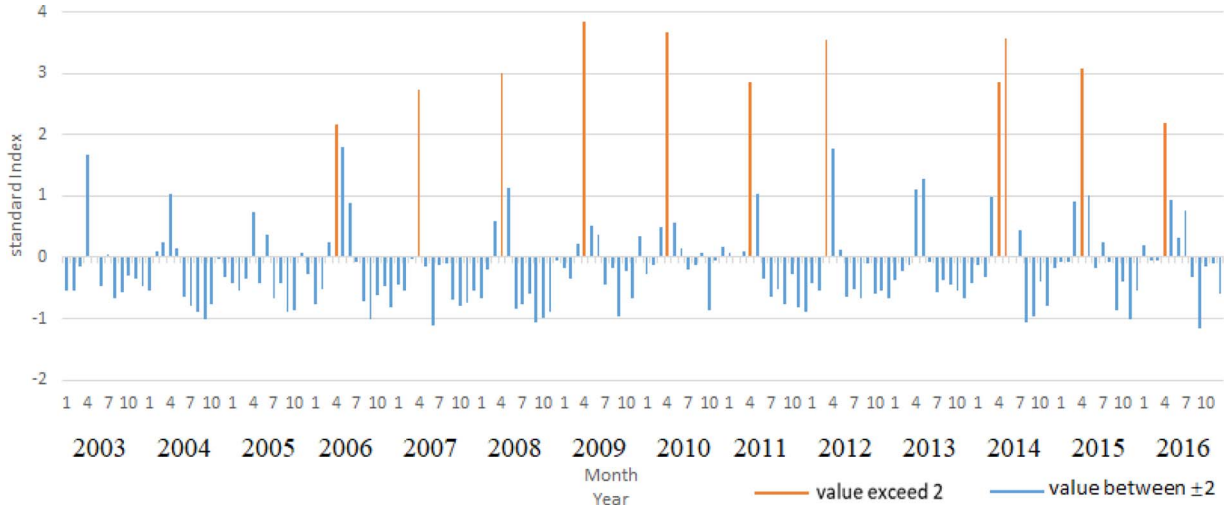

Fig. 5. Monthly DINEOF Chl-a concentration normalization index of 2003–2016.

the selected area was calculated as shown in Fig. 5. Taking $k_i = 2$ as the threshold, the high (low) value of the heat source is immediately apparent. As seen from Fig. 5, high months were April 2006, April 2007, April 2008, April 2009, April 2010, April 2011, March 2012, April and May 2014, April 2015, and April 2016. This indicates that there may be different extents of algae blooms in the springs of these years.

Fig. 6 shows the annual average of reconstructed SST for the ECS from 2003 to 2016. During the period, SST fluctuated along a slight upward trend. As the SST's trend was not passing the M–K test threshold of 95% confidence, this slight upward trend is not significant. Although the annual average SST values was changing from 21.6 °C to 22.8 °C, there was a downward trend during the period of 2007–2011, down to 21.6 °C in 2011, and then going upward to the peak value of 22.8 °C in 2016 (see Fig. 6).

Fig. 7 displays the monthly SST of the ECS during the entire annual cycle for these 14 years, with the temperature tracing a sine curve that reaches its maximum in summer and its minimum in winter. This portrays an obvious cyclical change of SST from 2003 to 2016.

Figs. 8 and 9 show that monthly reconstructed Chl-a and SST were temporally averaged to produce the monthly climatology for the study area. Overall, as a result of nutrient rich runoff from land via rivers, higher Chl-a concentrations are generally scattered along the coast and the estuary region, such as the Yangtze River estuary. Along the continental shelf, Chl-a variability is highest near shore and decreases with distance off shore, with its contours almost parallel to those of the coastline, much as reported by Nurdin et al. (2013) and Wu et al. (2008). Rainfall and river discharge markedly affected Chl-a concentration (Hendiarti et al., 2005). Observing the northeast area of the Yangtze River, we can see a tongue-like high-value area about 123°–126°E and 30°–33°N: The Yangtze River discharge contributes to it (Zhou et al., 2006; Wu et al., 2008).

Chl-a bloom is seen in spring (March, April, May) and reaches its maximum in April, with concentrations decreasing thereafter. Fig. 8 gives the monthly average SST and Chl-a concentrations in the ECS. As the yellow shows in the figure, April has the highest Chl-a concentration and September is the lowest. This result is consistent with the findings of previous studies (Zheng et al., 2012; Zheng and Hao, 2010). It also proved that the Chl-a concentration in the ECS is significantly affected by Kuroshio Front (Chu and Kuo, 2009; Siswanto et al., 2008; Shinya et al., 2016).

The climatological monthly composite of MODIS SST shown in Fig. 9 clearly presents spatial and temporal distribution of SST, by

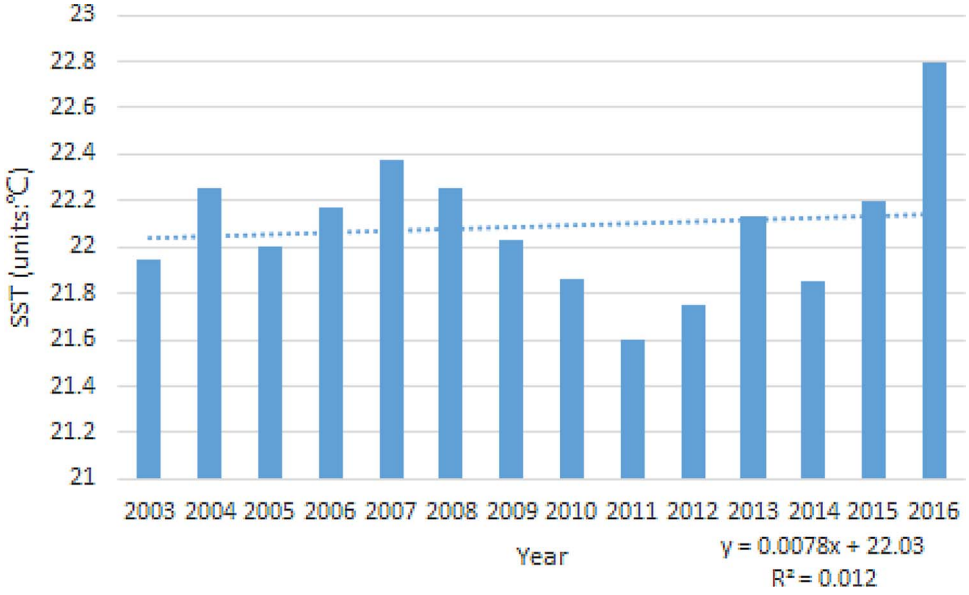

Fig. 6. Long-term changes of annual mean SST reconstructions from 2003 to 2016 (Z_c (SST) | < 1.64, the trend is insignificant, not passing the M-K test with the confidence of 95%).

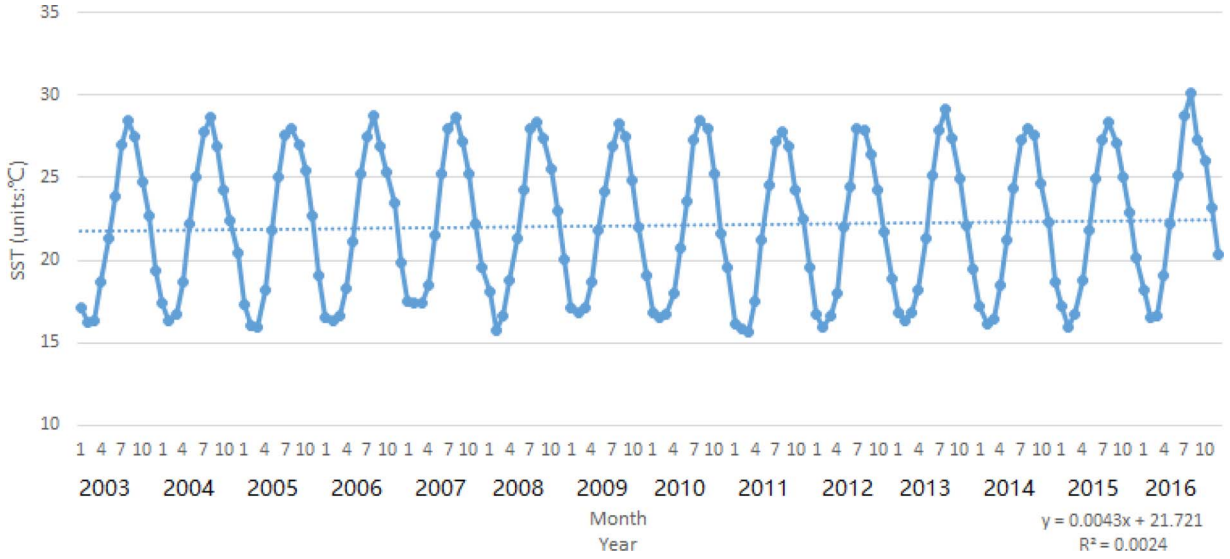

Fig. 7. Monthly DINEOF SST variation of the ECS from 2003 to 2016 (Z_c (DINEOF SST) | < 1.64, the trend is insignificant, not passing the M-K test with the confidence of 95%).

which the coastal areas and the region in the north of the ECS are characterized by obvious seasonal variations: these regions are shallow, and are subjected to river runoff. Comparatively speaking, SSTs in the southeast ECS show small changes—because some researchers claim that it is dominated by the warm Kuroshio Current (Xu et al., 2013). On the whole, SST increases with distance off shore, and the isotherms are nearly parallel to isobaths, running in the southeast direction, which is same as the previous findings (Gong and Wong, 2017). SST is varying seasonally (see Figs. 9 and 10): cold in winter (December, January, February) and spring (March, April, May), but warm in summer (June, July, August) and autumn (September, October, November). As reported by previous studies, the ECS SST is impacted by many factors, such as monsoons, tides, and river discharge (Kako et al., 2016; Johnson and Toy, 2017; Nurdin et al., 2013).

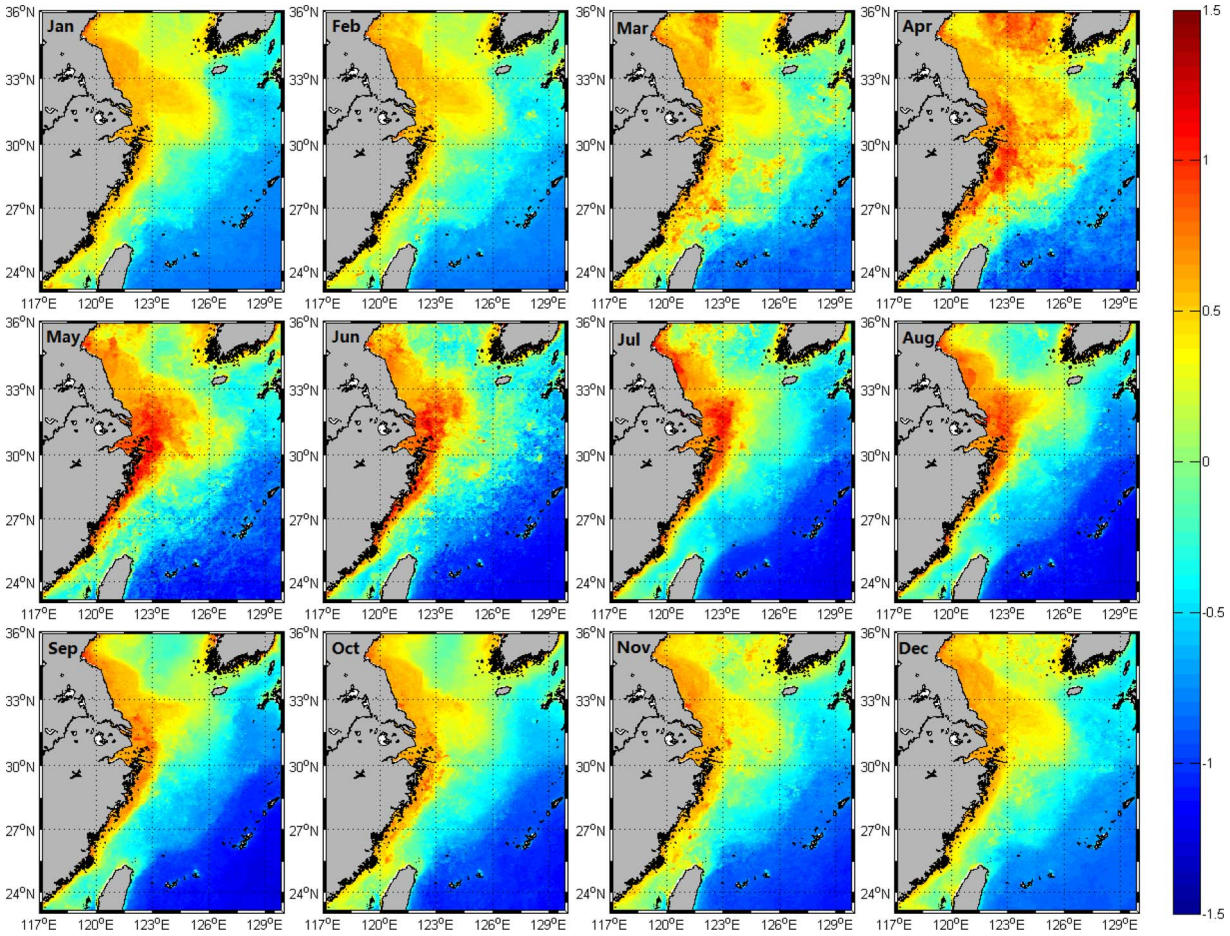

Fig. 8. Climatological monthly composite of MODIS Chl-a from 2003 to 2016 (The data were under the log-transformed).

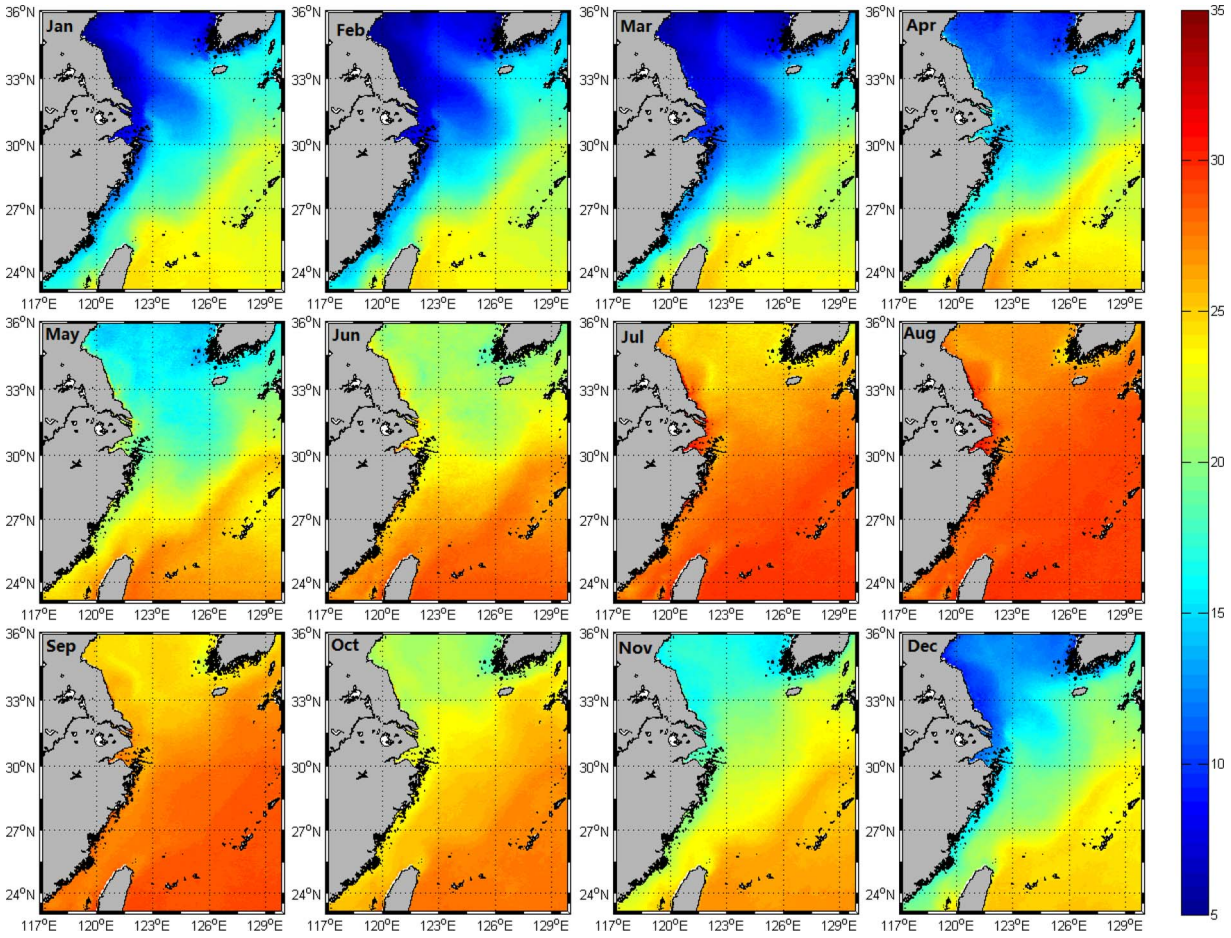

Fig. 9. Climatological monthly composite of MODIS SST from 2003 to 2016.

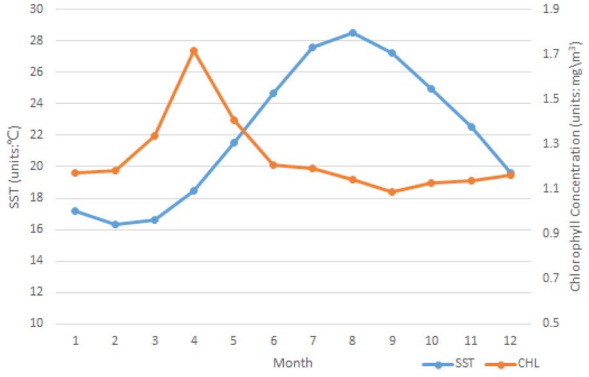

Fig. 10. Monthly climatologically average of SST and Chl-a concentration of the ECS.

3.2. Chl-a and SST correlations

To determine the relationship between Chl-a and SST, we calculated a correlation coefficient using the Chl-a and SST reconstruction data sets. Fig. 11 shows the correlation coefficient distribution for Chl-a and SST in the ECS during the period 2003–2016. Colored areas represent high correlation between the SST field and the Chl-a field, with correlation coefficients passing the *t*-test with a confidence level of 95%. Table 1 gives the correlation coefficient, SST, and Chl-a concentration for positive and negative correlated areas, respectively.

We used the SST and Chl-a of the regions of positive and negative correlations from Fig. 11 to make a scatter plot of the SST and Chl-a concentration (Fig. 12). As seen in Fig. 12a, there is a certain correlation between SST and Chl-a in the ECS, at $p < 0.05$, according to

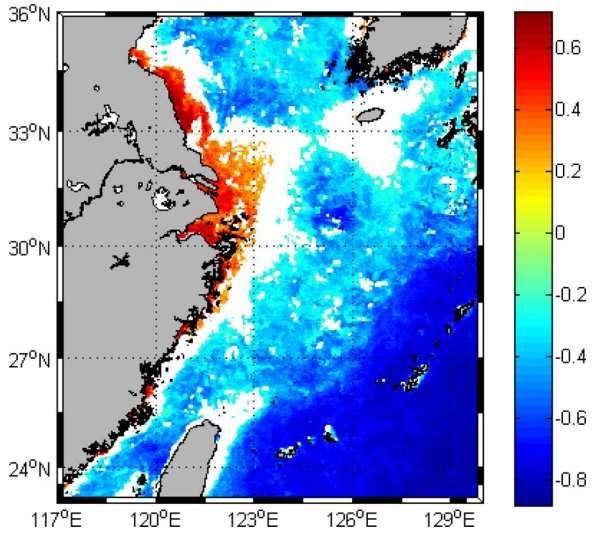

Fig. 11. Correlation between Chl-a and SST from 2003 to 2016 (the areas passing 95% significance test with color); before correlation analysis of SSTs and Chl-a time series, the data were de-trended.

Table 1. The coefficient of determination (R^2) is 0.3575 (for the positive correlated area) and 0.4605 (for the negative correlated area), respectively.

As shown in Fig. 11, the positive correlation area shows zonal distribution along the coastline. Especially in the north of Jiangsu Province, the Yangtze River estuary region, and the Hangzhou Bay, the

Table 1
The correlation coefficient of positive and negative area.

Area Parameter	positive	negative
Coefficient	0.3738	−0.499
Temperature (°C)	18.67	22.81
Chl-a concentration (mg/m^3)	4.53	0.79

correlation areas and coefficients are larger and higher than those of any other region where proximate to human-dominated landscapes. As shown in Table 1, the correlation coefficient of the positive area is 0.3738. For the mean surface temperature, it is only about 18.67 °C, whereas the concentration of Chl-a reaches up to 4.53 mg/m^3.

The southeast of the ECS shows a negative correlation between Chl-a and SST. The mean correlation coefficient of the negative area is −0.499, and the average temperature is about 22.81 °C. Compared with the positive area, the Chl-a concentration of the negative area is only 0.79 mg/m^3.

The regression of SST with Chl-a for the ECS (Fig. 13) also proves statistically significant correlations between SST and concentration of Chl-a. The areas of correlation in regression analysis are similar to the results in Fig. 11, illustrating the significant relationship of SST and Chl-a concentrations.

Fig. 14 gives the monthly average of SST and Chl-a concentration for the positive correlated areas shown in Fig. 11. As the yellow curve (Chl-a) in Fig. 14 shows, June has the highest Chl-a concentration and March is the lowest. The Chl-a concentration curve becomes steep from April to May, signifying the boom of chlorophyll in spring, whereas the sea surface temperature rises gradually. The mean temperature of the selected area is 19.53 °C and 23.29 °C in May and June, with the corresponding Chl-a concentrations 5.99 mg/m^3 and 6.19 mg/m^3, respectively.

4. Conclusions

In this study, SST and Chl-a data obtained through MODIS-Aqua were reconstructed using the DINEOF method, with a view to analyzing the relationship between the two variables of the ECS. This analysis has shown that Chl-a concentrations are highly correlated with sea surface temperature.

We applied the self-consistent DINEOF method to reconstruct 14 years' worth of satellite-derived (MODIS-Aqua) SST and Chl-a concentration data sets from the ECS. Compared with the raw data, the processed results fill in the gaps in the data, with their root mean square error reaching 0.4694 for SST and 0.5978 for Chl-a. The reconstructions present the distribution and variation trend of the two variables precisely, but the accuracy of the algorithm and the pretreatment process still needs to be refined in the future research.

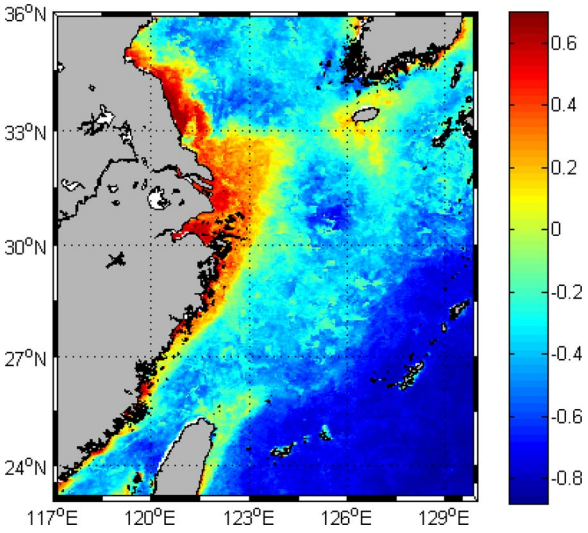

Fig. 13. Regression coefficients of SST with Chl-a for the period of 2003–2016 (the areas passed 95% significance test with color); the data were normalized before the correlation analysis of SST and Chl-a time series.

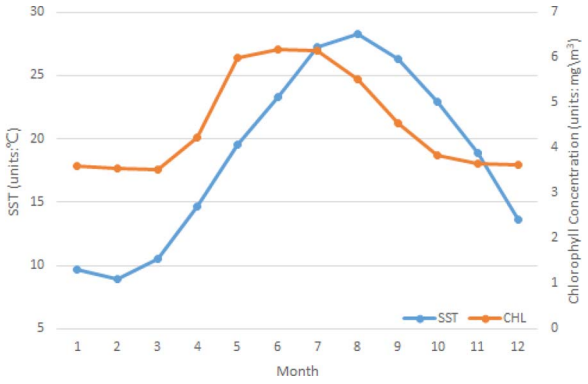

Fig. 14. Monthly climatologically average of SST and Chl-a concentration of the positive correlated areas in the ECS.

After the data preprocessing, a long-term change trend in Chl-a concentration from 2003 to 2016 was calculated. Chl-a concentration peaked in April–May and reached a low in July–August or, sometimes, in October–November. Peaks were evident in 2009, 2010, 2012, and 2014. The yearly mean shows a fluctuating upward trend in concentrations from 2003 to 2016. Analyzing the standard score of the whole monthly reconstruction Chl-a concentration, it is found that April 2006, April 2007, April 2008, April 2009, April 2010, April 2011, March 2012, April and May 2014, April 2015, and April 2016 were high

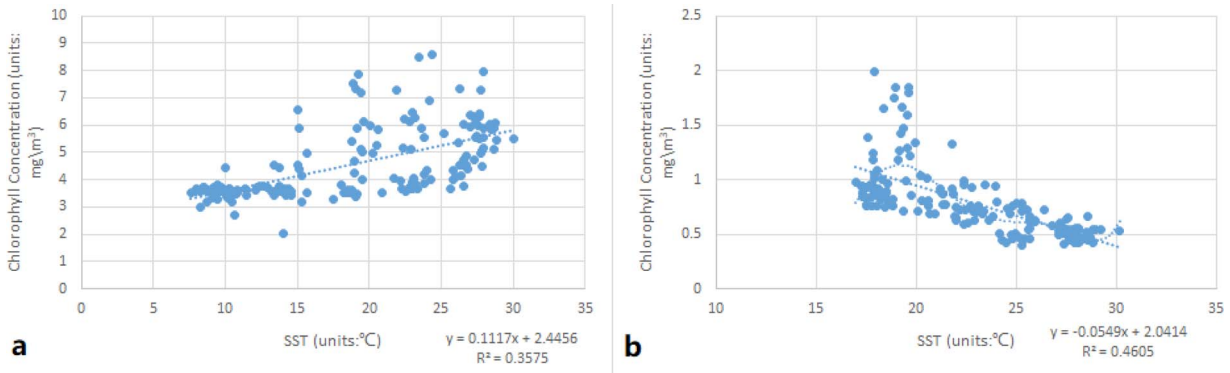

Fig. 12. Correlation scatter plot of the SST and Chl-a of the positive and negative correlated section in the ECS (2003–2016): (a) the positive correlation area, and (b) the negative correlation area, with the coefficient of determination (R^2) of 0.3575 and 0.4605, respectively.

times, which means the algae blooms in spring.

During the latest six years (2011–2016), the ECS SST has been risen continually, exhibiting notable interannual change marked by a summer maximum and winter minimum. From monthly climatology averages of Chl-a and SST, their spatial distribution characteristics are clear. Along the continental shelf, Chl-a variability is highest near shore and decreases with distance off shore, almost paralleling to the coastline. Especial in the Yangtze River estuary, its values are higher than elsewhere, indicating that river discharge markedly affects Chl-a concentrations. What's more, Chl-a booms can be seen in spring. In comparison, the SST displays nearly the opposite trend. The shallow topography of coastal areas and the north of the ECS is characterized by large seasonal variations in SST.

Through correlation and regression analysis, we found that SST in the coastal area (such as in the north coast of Jiangsu Province, in the Yangtze River estuary region, and in the Hangzhou Bay) appreciably affected Chl-a concentration, exhibiting a positive correlation. Especially from April to June, concentrations of Ch-a increased sharply with increases in SST—the same time when red tides frequently occur. The mean temperature of these three months is 19.16 °C. For the southeast of the ECS, the relationship between SST and Chl-a concentration is negative, but the specific relationship between them is not clear. It is probably the low nutrient concentration that leads to it, or it is very possible that the excessive temperature inhibits the growth of phytoplankton.

Although the present work shows that Chl-a concentrations are significantly affected by SST, previous studies indicated that certain other factors should also be taken into account. These can include sea surface salinity (SSS), surface flow zones, oxygen abundance, and temperature gradients. But such factors will be addressed in the study area in the near future.

Acknowledgments

The data from NASA's Ocean Biology Processing Group for providing MODIS Aqua/Terra, Level 3 (4-km equi-rectangular projection) daily for Chl-a and Sea surface temperature (SST), NASA Web SeaDAS development group for providing Ocean Colour SeaDAS Software for processing Chl-a and SST data and Remote Sensing Systems are highly appreciated. The research is jointly supported by the National Key Research and Development Program of China (2016YFC1402003), the State Key Lab Fund for Geological Processes and Mineral Resources (2016), the "2015 Innovation Program for Research and Entrepreneurship Teams, Jiangsu Province, China" and the Priority Academic Program Development of Jiangsu Higher Education Institutions (PAPD).

References

Alvera-Azcárate, A., Barth, A., Rixen, M., Beckers, J.M., 2005. Reconstruction of incomplete oceanographic data sets using empirical orthogonal functions: application to the adriatic sea surface temperature. Ocean Model. 9, 325–346.

Bao, B., Ren, G., 2014. Climatological characteristics and long-term change of SST over the marginal seas of China. Cont. Shelf Res. 77, 96–106.

Barber, Richard T., Chavez, Francisco P., 1983. Biological consequences of El Niño. Science 222, 1203–1210.

Beckers, J.M., Rixen, M., 2003. EOF calculations and data filling from incomplete oceanographic datasets. J. Atmos. Oceanic Technol. 20, 1839–1856.

Chaturvedi, N., 2005. Variability of chlorophyll concentration in the Arabian Sea and Bay of Bengal as observed from SeaWiFS data from 1997 to 2000 and its interrelationship with Sea Surface Temperature (SST) derived from NOAA AVHRR. Int. J. Remote Sens. 26 (17), 3695–3706.

Chu, Peter C., Kuo, Yu-heng, 2009. Biophysical variability in the kuroshio extension from altimeter and SeaWiFS. IEEE/MTS Oceans.

Colwell, R.R., 1996. Global climate and infectious disease: the cholera paradigm. Science 274 (5295), 2025–2031.

Fei, W., Sun, X.X., Shan, Z., 2012. Spatial and seasonal variations of chlorophyll a and primary productivity in spring and summer in the yellow sea and east china sea. Oceanol. Limnol. Sin. 43 (3), 438–444.

Gong, S., Wong, K., 2017. Spatio-Temporal Analysis of Sea Surface Temperature in the East China Sea Using TERRA/MODIS Products Data, Sea Level Rise and Coastal Infrastructure. InTech, Croatia (In press).

Gong, G.C., Chen, Y.L.C., Liu, K.K., 1996. Chemical hydrography and chlorophyll a distribution in the East China Sea in summer: implications in nutrient dynamics. Cont. Shelf Res. 16 (22), 1561–1590.

Gong, G.C., Wen, Y.H., Wang, B.W., Liu, G.J., 2003. Seasonal variation of chlorophyll a concentration, primary production and environmental conditions in the subtropical East China Sea. Deep-Sea Res. II 50, 1219–1236.

Hartmann, D.L., Michelsen, M.L., 1989. Intraseasonal peridiocities in indian rainfall. J. Armos. Sci. 46 (18), 2838–2862.

Hendiarti, N., Suwarso, E., Aldrian, K., Amri, R., Andiastuti, S., Sachoemar, I., Wahyono, I.B., 2005. Seasonal variation of pelagic fish catch. J. Oceanogr. 18 (4), 112–123.

Jacox, M.G., Hazen, E.L., Zaba, K.D., Rudnick, D.L., Edwards, C.A., Moore, A.M., Bograd, S.J., 2016. Impacts of the 2015–2016 El Niño on the California Current System: early assessment and comparison to past events. Geophys. Res. Lett. 43.

Jiao, N., Zhang, Y., Zeng, Y., 2007. Ecological anomalies in the east China sea: impacts of the three Gorges dam? Water Res. 41 (41), 1287–1293.

Johnson, Richard H., Toy, Michael D., 2017. SST Gradients and the East Asian Early-Summer Monsoon, The Global Monsoon System: Research and Forecast. (chapter 1).

Jutla, A.S., Akanda, A.S., Griffiths, J.K., et al., 2011. Warming oceans, phytoplankton, and river discharge: implications for cholera outbreaks. Am. J. Trop. Med. Hyg. 85 (2), 303–308.

Kako, S., Nakagawa, T., Takayama, K., Hirose, N., Isobe, A., 2016. Impact of Changjiang River discharge on sea surface temperature in the East China Sea. J. Phys. Oceanogr.

Kavak, M.T., Karadogan, S., 2011. The relationship between sea surface temperature and chlorophyll concentration of phytoplanktons in the Black Sea using remote sensing techniques. J. Environ. Biol. 32, 493–498.

Kendall, G., 1975. 4th ed. Rank Correlation Methods, vol. 4. Charles Griffin, London, UK, pp. 202.

Lee, K.-W., Yeh, S.-W., Kug, J.-S., Park, J.-Y., 2014. Ocean chlorophyll response to two types of El Niño events in an ocean-biogeochemical coupled model. Geophys. Res. Oceans 119, 933–952.

Lobitz, B., Beck, L., Huq, A., et al., 2000. Climate and infectious disease: use of remote sensing for detection of Vibrio cholerae by indirect measurement. Proc. Natl. Acad. Sci. 97 (4), 1438–1443.

Mann, B., 1945. Non-parametric tests against trend. Econometrical 13, 163–171.

Mati, K., Mitchell, B.G., 2000. Influence of the 1997–98 El Nifio on the surface chlorophyll in the California Current. Geophys. Res. Lett. 27 (18), 2937–2940.

Miles, Travis N., He, Ruoying, 2010. Temporal and spatial variability of Chl-a and SST on the South Atlantic Bight: revisiting with cloud-free reconstructions of MODIS satellite imagery. Cont. Shelf Res. 30, 1951–1962.

Nakamoto, S., Kumar, S.P., Oberhuber, J.M., Ishizaka, J., Muneyama, K., Frouin, R., 2001. Response of the equatorial Pacific to chlorophyll pigment in a mixed layer isopycnal ocean general circulation model. Geophys. Res. Lett. 28, 2021–2024.

Nurdin, S., Mustapha, M.A., Lihan, T., 2013. The relationship between sea surface temperature and chlorophyll-a concentration in fisheries aggregation area in the archipelagic waters of spermonde using satellite images. J. Am. Inst. Phys. 1571, 466–472.

Park, J.Y., Kug, J.S., Park, J., Yeh, S.W., Jang, C.J., 2011. Variability of chlorophyll associated with El Niño–Southern Oscillation and its possible biological feedback in the equatorial Pacific. J. Geophys. Res. 116, C10001.

Pearson, K., 1895. Notes on regression and inheritance in the case of two parents. Proc. R. Soc. Lond. 58, 240–242.

Shinya, Kouketsu, Hitoshi, Kaneko, Takeshi, Okunishi, Kosei, Sasaoka, Sachihiko, Itoh, Ryuichiro, Inoue, Hiromichi, Ueno, 2016. Mesoscale eddy effects on temporal variability of surface chlorophyll a in the Kuroshio Extension. J. Oceanogr. 72, 439–451.

Siswanto, E., Nakata, H., Matsuoka, Y., Tanaka, K., Kiyomoto, Y., Okamura, K., Zhu, J.R., Ishizaka, J., 2008. The long-term freshening and nutrient increases in summer surface water in the northern East China Sea in relation to Changjiang discharge variation. J. Geophys. Res. 113, C10030.

Steidinger, K.A., Haddad, K.D., 1981. Biologic and hydrographic aspects of red tides. Bioscience 31, 814–819.

Tang, X., Wang, F., Chen, Y., et al., 2009. Warming trend in northern East China Sea in recent four decades. Chin. J. Oceanol. Limnol. 27 (2), 185–191.

Thomas, A.C., Carr, M.E., Strub, P.T., 2001. Chlorophyll variability in eastern boundary currents. Geophys. Res. Lett. 28 (18), 3421–3424.

Tomlinson, M.C., Stumpf, R.P., Ransibrahmanakul, V., Truby, E.W., Kirkpatrick, G.J., Pederson, B.A., 2004. Evaluation of the use of SeaWiFS imagery for detecting Karenia brevis harmful algal blooms in the eastern Gulf of Mexico. Remote Sens. Environ. 91, 293–303.

Tran, A.V., Simith, E., Hyon, J., Evans, R., Brown, O., Feldman, G., 1993. Satel Lite-derived Multichannel Sea Surface Temperature and Phytoplankton Pigment Concentration Data: A CD-ROM Set Containing Monthly Mean Distributions for the Global Oceans. Jet Propulsion Laboratory, Pasadena, CA.

Tseng, C., Lin, C., Chen, S., et al., 2000. Temporal and spatial variations of sea surface temperature in the East China Sea. Cont. Shelf Res. 20 (4), 373–387.

Wang, Y.Q., Liu, D.y., 2014. Reconstruction of satellite chlorophyll-a data using a modified DINEOF method: a case study in the Bohai and Yellow seas, China. Int. J. Remote Sens. 35:1, 204–217.

Wang, T.Y., Mao, Z.H., Gong, F., 2010. The study on the correlation between the sea surface temperature and chlorophyll of Zhejiang coastal by the satellite remote sensing image. International Conference on Remote Sensing.

Wu, Y.M., Xu, Z.L., Cui, X.S., Fan, W., 2008. Temporal-spatial change of concentration of chlorophyll-a in the east China sea during 1997–2007. J. Res. Environ. Sci. 21 (6), 137–142.

Xu, Y.J., Joji, Ishizaka, Hisashi, Yamaguchi, Eko, Siswanto, Shengqiang, Wang, 2013. Relationships of interannual variability in SST and phytoplankton blooms with

giantjellyfish (Nemopilema nomurai) outbreaks in the Yellow Sea and East China Sea. J. Oceanogr. 5 (69), 511–526.
Yang, H., He, C.L., 2009. The red tide events in the china sea and the relationship with the temperature and El Niño. J. Trans. Oceanol. Limnol. 2, 1–6.
Yue, S., Wang, C.Y., 2004. The Mann–Kendall test modified by effective sample size to detect trend in serially correlated hydrological series. Water Resour. Manage. 18 (3), 201–218.
Zhang, J., Liu, S.M., Ren, J.L., Wu, Y., Zhang, G.L., 2007. Nutrient gradients from the eutrophic Changjiang (Yangtze River) Estuary to the oligotrophic Kuroshio waters and reevaluation of budgets for the East China Sea Shelf. Prog. Oceanogr. 74 (4), 449–478.
Zhang, Y., Huang, Z., Fu, D., Tsou, J.Y., Jiang, T., Liang, X.S., Lu, X., 2017. Monitoring of chlorophyll-a and sea surface silicate concentrations in the south part of Cheju island in the East China Sea using MODIS data. Int. J. Appl. Earth Obs. Geoinf (in this special issue).
Zheng, X.S., Hao, W., 2010. Seasonal and interannual variability of chlorophyll in the east China sea. J. IEEE 10, 2653–2656.
Zheng, X.S., Wei, H., Wang, Y.H., 2012. Seasonal and inter-annual variations of chlorophyll-a concentration based on the remote sensing data in the yellow sea and east china sea. J. Oceanol. Limnol. Sin. 43 (3), 649–654.
Zhou, J.L., Liu, Z.T., Meng, W., Li, Z., Li, J., 2006. The characteristics of nutrients distribution in the Yangtze River estuary. Res. Environ. Sci. 6 (19), 139–144.
Zill, D., Wright, S., Cullen, M.R., 2011. Advanced Engineering Mathematics, 4th ed. Jones and Bartlett Publishers, Sudbury, Massachusetts.